J. Membrane Biol. 98, 257–274 (1987)

The Journal of
Membrane Biology

Electrical Characteristics of Stomatal Guard Cells: The Contribution of ATP-Dependent, "Electrogenic" Transport Revealed by Current-Voltage and Difference-Current-Voltage Analysis

Michael R. Blatt
Botany School, University of Cambridge, Cambridge CB2 3EA, England

Summary. The steady-state, current-voltage (*I-V*) characteristics of stomatal guard cells from *Vicia faba* L. were explored by voltage clamp using conventional electrophysiological techniques, but with double-barrelled microelectrodes containing 50 mM K^+-acetate. Attention was focused, primarily, on guard cell response to metabolic blockade. Exposures to 0.3–1.0 mM NaCN and 0.4 mM salicylhydroxamic acid (SHAM) lead consistently to depolarizing (positive-going) shifts in guard cell potentials (V_m), as large as +103 mV, which were generally complete within 60–90 sec (mean response half-time, 10.3 ± 1.7 sec); values for V_m in NaCN plus SHAM were close or positive to −100 mV and well removed from the K^+ equilibrium potential. Guard cell ATP content, which was followed in parallel experiments, showed a mean half-time for decay of 10.8 ± 1.9 sec ($[ATP]_{t=0}$, 1.32 ± 0.28 mM; $[ATP]_{t=60-180sec}$, 0.29 ± 0.40 mM). In respiring cells, the *I-V* relations were commonly sigmoid about V_m or gently concave to the voltage axis positive to V_m. Inward- and outward-rectifying currents were also observed, especially near the voltage extremes (nominally −350 and +50 mV). Short-circuit currents (at $V = 0$ mV) were typically about 200–500 mA m^{-2}. The principal effect of cyanide early on was to linearize the *I-V* characteristic while shifting it to the right along the voltage axis, to decrease the membrane conductance, and to reduce the short-circuit current by approx. 50–75%. The resulting difference-current-voltage (*dI-V*) curves (±cyanide) showed a marked sensitivity to voltages negative from −100 mV and, when clamp scans had been extended sufficiently, they revealed a distinct minimum near −300 mV before rising at still more negative potentials. The difference currents, along with changes in guard cell potential, conductance and ATP content are interpreted in context of a primary, ATP-consuming ion pump. Fitting *dI-V* curves to reaction kinetic model for the pump [Hansen, U.-P., et al. (1981) *J. Membrane Biol.* **63**:165; Blatt, M.R. (1986) *J. Membrane Biol.* **92**:91] implicates a stoichiometry of one (+) charge transported outward for each ATP hydrolyzed, with pump currents as high as 200 mA m^{-2} at the free-running potential. The analysis indicates that the pump can comprise more than half of the total membrane conductance and argues against modulations of pump activity alone, as an effective means to controlling K^+ transport for stomatal movements.

Key Words stomatal guard cell · (difference-) current-voltage relation · conductance-voltage relation · H^+ pump · kinetic carrier model · K^+ transport · *Vicia*

Introduction

Stomatal guard cells of higher plant leaves are remarkable for their ability to accumulate and lose K^+ (and to a lesser extent, Cl^-) ions under the influence of light, CO_2, phytohormones and fungal toxins. This capability plays a fundamental role in the osmotically-driven processes of stomatal opening and closure (*see* Raschke, 1979; Outlaw, 1983; for reviews). It presents, also, a unique opportunity in which to examine membrane transport in a higher plant cell. Movements of solutes across guard cell membranes are likely to occur by mechanisms common to other higher plant cells, algae and fungi.

Attention to the electrophysiological properties of guard cells has been drawn, in particular, by recent studies of protoplasts using novel patch electrode methods (Schroeder, Hedrich & Fernandez, 1984; Assmann, Simoncini & Schroeder, 1985). Far from clarifying the strategies for K^+ transport and its regulation in stomatal movements, however, these studies have heightened awareness of how unsatisfactory our current understanding is of guard cell, and generally of higher plant cell transport physiology. Conventional wisdom maintains that K^+ transport in higher plant cells is primarily dissipative, driven by the prevailing electrochemical potential (thermodynamic) gradient for the ion. Elaborating on this concept, Zeiger (1983) has suggested that control, both of the magnitude and of the direction, for net K^+ movements in guard cells could come from modulating primary "electrogenic" pump activity against the background of a K^+ channel.

The two patch electrode studies of *Vicia* guard cell protoplasts—and correlative evidence from light- and fusicoccin-induced medium acidifications (Gepstein, Jacobs & Taiz, 1982; Shimazaki, Iino & Zeiger, 1986)—appear to support this notion. None-

theless, a quantitative assessment must raise some doubts. In particular, the light-induced currents recorded (Assmann et al., 1985) were extraordinarily small, either in comparison with those of other plant and fungal cell types (Beilby 1984; Slayman & Sanders 1985; Takeshige, Shimmen & Tazawa, 1986) or in relation to estimates of guard cell respiration (Shimazaki et al., 1983). Also, net H^+ extrusion rates, the light-induced currents, and estimates of K^+ uptake for stomatal opening (*see* MacRobbie, 1987, for review) are remarkably similar; the comparison seems to imply that *all* primary H^+ transport is devoted to cation (H^+/K^+) exchange and that secondary transport processes are overwhelmingly dominated by the K^+ diffusion regime. Indeed, the "pump-and-channel" model obviates the very mechanism by which K^+ *loss* is proposed to occur, that is, by a shift in the membrane potential to values *positive* of the K^+ equilibrium potential (E_K). As MacRobbie (1981, 1983, 1987) has pointed out, controlling a primary pump alone simply is not sufficient to account for much of stomatal behavior.

A second, but related, issue is the voltage sensitivity of the pump itself. For guard cells, as for higher plant cells generally, the voltage-dependent characteristics of the pump remain unexplored. In two model cell types—*Neurospora* and *Chara*—primary ion (H^+) pumping shows a marked response to membrane potential, even at voltages well removed from the pump equilibrium potential (E_p). This fact, along with changes in pump kinetic characteristics with pH (Beilby, 1984; Slayman & Sanders, 1985), has contributed to an understanding both of mechanisms for pump control and of the kinetic relationships between the pump and H^+-coupled secondary transport (*see* Hansen & Slayman, 1978 [*but also* Blatt, 1986]; Sanders, Hansen & Slayman, 1981; Blatt & Slayman, 1987).

Understanding the patterns of solute transport and their regulation, in fungi, in algae and in higher plant cells alike, depends not only on identifying the relevant transport processes, but also on a secure knowledge of their kinetic properties. In this respect, guard cells offer one enormous advantage over most other higher plant cell types. Because guard cells are isolated from their neighboring epidermal and mesophyll cells in situ (Wille & Lucas, 1984; Palevitz & Hepler, 1985), the voltage-dependent characteristics of the cells are not compromised by uncertainties about current distribution over the membrane, and currents can be related to the membrane surface area directly.

This paper builds on a previous study (Blatt, 1987*a*) which described the ionic basis of the guard cell potential[1] and the effects of microelectrode salt leakage. I explore the voltage-dependent characteristics of the guard cells and contributions made by primary "electrogenic" ion transport, as revealed through metabolic blockade with cyanide, voltage clamping and current-voltage (*I-V*) analysis. The results are consistent with the idea of a proton pump (H^+-ATPase) operating at the guard cell plasma membrane. They support a unitary charge stoichiometry [1(H^+) : 1(ATP)], and indicate that the pump can contribute appreciably both to the membrane conductance and to the membrane potential, even when the free-running potential is positive of E_K.

Materials and Methods

Plant Culture and Experimental Protocol

Vicia faba L., cv. (Bunyan) Bunyard Exhibition, was grown hydroponically in Hoagland's Salts medium between April and June, 1986, and epidermal strips were prepared as described before (Blatt, 1987*a*). All measurements were carried out in 5 mM Ca^{2+}-HEPES,[2] pH 7.4 [5 mM HEPES buffer titrated to pH 7.4 with $Ca(OH)_2$], with 0.1 mM KCl (final $[Ca^{2+}] \simeq 1$ mM). Ambient temperatures were 20–22°C. Cyanide was added as the sodium salt to give a final concentration of 0.3 or 1.0 mM, and in most experiments 0.4 mM salicylhydroxamic acid (SHAM) was included to block alternate oxidase pathways for electron transport. As in the previous study (Blatt, 1987*a*), the solutions were added at one end of the experimental chamber and removed by aspiration at the other end. A continuous flow of medium (approx. 10 chamber vol/min) was maintained throughout each experiment. Cells were challenged with the inhibitors, on several occasions, under green background lighting from the microscope lamp [AL554 interference filter (Schott, Mainz, FRG), 23 nm half bandwidth; incident light calculated at 554 nm, 2 μmol $m^{-2}sec^{-1}$], but the practice was discontinued when analogous results were recorded with low-intensity white light (50 μmol $m^{-2}sec^{-1}$ photosynthetically active irradiation).

Surface areas and volumes were calculated assuming a cylindrical geometry, and the orthogonal dimensions (diameter, length) of impaled cells were measured with a calibrated eyepiece micrometer.

Electrical

Electrode manufacture, KCl|Ag-AgCl halfcell construction and mechanical operations have been described in detail (Blatt &

[1] For reasons detailed previously (Blatt, 1987*a*), electrical recordings from the guard cells are thought to reflect the characteristics of the plasma membrane. I use the terms guard 'cell' and 'membrane' potential and conductance in this context.

[2] *Abbreviations:* HEPES, 4-(2-hydroxyethyl)-1-piperazine ethanesulfonic acid; SHAM, salicylhydroxamic acid; V_m, (free-running) membrane potential; G_m, membrane slope conductance at V_m; (*d*)*I-V*, (difference) current-voltage (relation); *G-V*, slope conductance-voltage (relation).

Slayman, 1983; Blatt, 1987*a*). Electrodes were filled with a 50-mM K^+-acetate electrolyte to minimize microelectrode salt leakage and salt-loading artifacts (Blatt & Slayman, 1983; Blatt, 1987*a*). The electrolyte was prepared by titrating an acetic acid solution to pH 7.2 with KOH. Most recordings were obtained by the two-electrode method using double-barrelled microelectrodes. One barrel was used for passing current, while the second barrel monitored the membrane potential (*see* Fig. 1*A*; also Blatt, 1987*a*). In one series of experiments (Appendix), measurements were carried out using a second, single microelectrode placed distally within the cell. In these experiments, the additional electrode and preamplifier (below) were mounted on a second Huxley-type micromanipulator (Goodfellow Metals, Cambridge) for positioning, but impalements were achieved by advancing the *cell* on the two (double- and single-barrelled) electrode tips using the microscope stage micrometer movement.

Current-voltage relations were obtained by voltage clamp. The clamp was driven by, and electrometer current and voltage outputs were monitored under the control of an IBM-PC microcomputer, equipped with a 12-bit, 30 kHz analog-to-digital converter (AD) and multiplexer, and two digital-to-analog (DA) converters (Tecmar, Cleveland, OH). Data logging, display, analysis and storage were accomplished using a single, multitask program running under 512 Kbytes of memory and designed to drive 348 × 720 screen- (Hercules Computer Technology, Berkeley, CA) and 576 × 576 printer-matrix (Epson, Nagano, Japan) graphics. (The program, with Fortran and Assembler source coding, is available on request.)

Figure 1*A* shows a schematic of the analog circuitry and digital linkup. Cell potentials were recorded by a set of custom-built, electrometer amplifiers, each equipped with a shielded and driven preamplifier (input impedance $>2 \times 10^{12}$ Ω), a bootstrap circuit for passing current and trimming capacitative compensation (0-100 pF).

The voltage clamp comprised an LF355 operational amplifier (National Semiconductor), configured as a comparator, with a 10 MΩ feedback for a gain of 200. In tests with 1 GΩ · 10 pF path to ground, the trimmed clamp circuit showed settling times <200 μsec (command voltage steps, 0.1–0.5 V, <10 μsec rise time). A current clamp, used in the previous study (Blatt, 1987*a*), was driven from DA_1 directly.

Clamp currents normally were monitored at the clamp (voltage) output, but were found to be independent of electrode resistance and free from rectification (Blatt, 1987*a*). For sampling, the current output was filtered by a four-pole Bessel filter [nominal f_c (−3 dB), 3 kHz or, for steady-state *I-V* scans, 1 kHz]. All AD inputs and DA outputs were driven differentially to minimize pickup, and analog and digital grounds were separated.

To determine the steady-state *I-V* relations of the guard cells, a bipolar staircase of command voltages was used to drive the membrane alternately positive and negative from the free-running potential (Fig. 1*B*). The voltage steps were separated by equivalent periods, during which the membrane was clamped to the free-running potential. The entire staircase generally comprised 20 (±) pairs of command pulses distributed between this potential and two preset limits (usually −350 or −400 mV, and +50 or +100 mV). Command pulses were typically set for 100-msec duration and the AD inputs were sampled during the final 10 msec (or 20 msec for digital ac filtering) of each pulse. Thus, an entire scan, with 20 pairs of 100-msec long pulses, required 8 sec; but this time could be shortened by reducing the number of pulses or by shortening the pulse length.

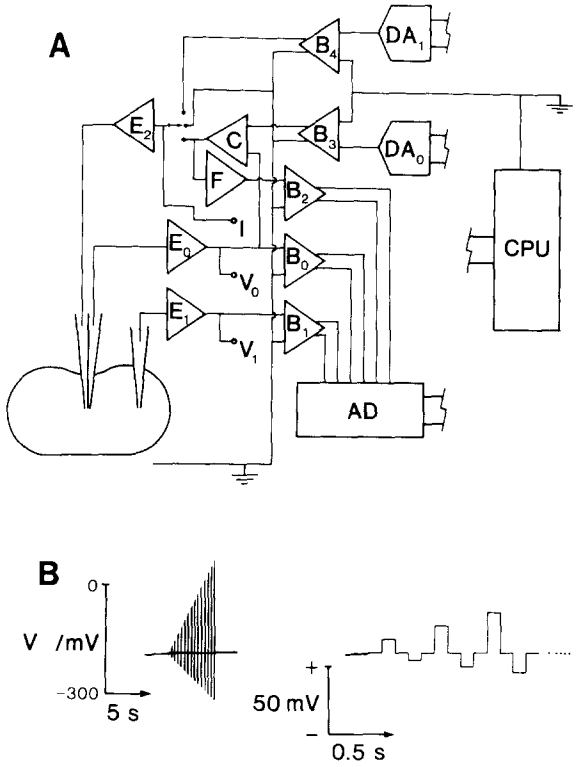

Fig. 1. Analog circuitry and digital linkup (*A*) and schematics of the voltage clamp scan (*B*). (*A*) Membrane potentials were followed with electrometers E_0 and E_1. Electrometer E_2 was dedicated to current injection for voltage- or for current-clamping, as dictated by a digital switch and the selected signal driver. The voltage clamp comprised E_0, a voltage comparator (*C*) and a four-pole Bessel filter (*F*). One digital-to-analog converter (DA_0) was dedicated to drive the clamp comparator. A second converter (DA_1) was used for current clamping. Membrane potentials and currents (voltage signal) were taken at points V_0, V_1 and *I* for output to oscilloscope and chart recorder. The signals were recorded also with a single analog-to-digital converter and multiplexer (*AD*) operating differentially. Analog and digital grounds were separated through a bank of unity-gain, differential amplifiers (B_0–B_4). (*B*) Schematic (left) shows typical time course and range for a voltage-clamp staircase, and on an expanded time scale (right). *See also* Fig. A1

Time-dependent features of clamp currents and voltages were obtained by recording current and voltage signals alternately at preset frequencies selectable between 0.01 and 10 kHz (nominally 1 kHz) and during selected clamp pulses. For these measurements, the clamp was driven, in turn, through a series of pulse cycles, each incorporating up to four, independently-programmable pulse steps.

Both time-dependent and steady-state, current and voltage data were subjected to preliminary analysis (cell geometry, amplifier calibrations), optionally plotted on screen, and then stored, with relevant recording parameters, on disk for later examination. Screen plots could be accumulated, also, bit-mapped in memory for immediate comparisons of successive clamp scans during an experiment, or for output to a dot-matrix printer.

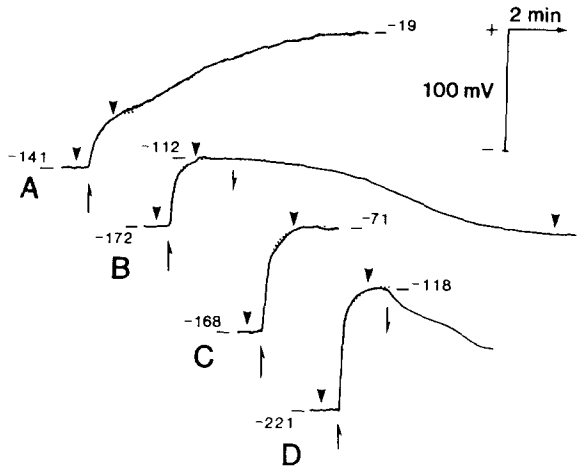

Fig. 2. Membrane potential response to NaCN and SHAM in four guard cells. Cyanide (0.3 mM, *A*; 1.0 mM, *B–D*) and 0.4 mM SHAM added (↑) and removed (↓ , *B, D*) as indicated. Current-voltage scans (masked from the traces) were run at times marked by the carats above each trace. Dotted lines are fittings to a single falling exponential (*see* Results). Traces *B* and *D* correspond to the data sets in Figs. 5 and 9, respectively

ATP

Guard cell ATP pools were determined by luciferin-luciferase assay, in a modification of the method described by Scott and Ellar (1978). Three to four young, fully-expanded leaves from a single plant were selected and stripped of the adaxial epidermis. The epidermal strips were floated on 5 mM Ca^{2+}-HEPES with 0.1 mM KCl, trimmed to roughly uniform size (1 cm^2), and were sonicated (Shimazaki, Gotow & Kondo, 1982; Shimazaki et al., 1983) to remove adhering mesophyll cells and to kill the epidermal cells. After sonicating, the strips were divided into lots of 6–8 and were photographed (Tech Pan, Kodak, Hemell Hempstead, UK) to record surface areas and stomatal densities. The strips were then set aside for 2 hr before proceeding. At this time, and during the treatments (below), the lots were kept at 20–22°C under room lighting (incident photosynthetically active irradiation, 10 μmol m^{-2} sec^{-1}). [Visual checks with Nomarski D.I.C. optics (160× and 400×, Universal, Zeiss, Oberkochen, FRG) showed that limited sonication was sufficient to remove or destroy all of the mesophyll and epidermal cells. At the same time, greater than 90% of the guard cells survived the treatment, even 24 hr after sonicating. They retained the fine granular appearance of the cytoplasm, cytoplasmic streaming of small organelles, and a normal distribution of chloroplasts and of the nucleus.]

Experiments were begun by transferring strips from each lot to a 1.5-ml microfuge tube and, at time zero, adding to the tube 1.0 ml of 5 mM Ca^{+}-HEPES, 0.1 mM KCl with or without 1.0 mM NaCN and/or 0.4 mM SHAM, and then agitating the tube by vortexing for 5 sec. At various times thereafter, the solution was removed by aspiration and the treatment was terminated by adding 1.0 ml of boiling propan-2-ol (85°C). The tube was vortexed again briefly, and was then set in an 85°C water bath for 10 min. Finally, the lots were frozen in liquid nitrogen and freeze-dried at −40°C.

Luciferin-luciferase assays were carried out with Tris-aspartate buffered reagents (Sigma, St. Louis, MO). The lots were rehydrated in 0.5 ml of 50 mM Tris-aspartate, pH 7.75, vortexed and then centrifuged at 1000 × *g* to pellet cell wall debris. ATP-dependent luminescence was followed over time with an LKB Wallac 1250 Luminometer (LKB, Stockholm) and strip chart recorder. The magnitude of the luminescence peak, which occurred roughly 2 sec after adding the reagents, was used to quantitate the signal. Calibrations were carried out with equivalent buffer volumes containing 0.2–100 pmol ATP. Over this range the signal was linear with ATP content. Typical signals from the lot samples were between 1 and 10 pmol ATP. Internal standards, which were added to selected lots or included separately at extraction times, indicated yields for ATP of 82–95%.

Numerical Analysis

Cell potentials and ATP contents in the presence of NaCN and SHAM were fitted by a nonlinear, least-squares algorithm (Marquardt, 1963) to a single falling exponential of the form

$$y = p_1 - p_2/e^{p_3 x}. \quad (1)$$

In both cases, fittings were carried out after normalizing the respective data points in each set to the controls (−NaCN, −SHAM).

Preliminary analyses of the guard cell *I-V* relations and derivations of difference-current-voltage (*dI-V*) curves, likewise, made use of the nonlinear, least-squares algorithm, fitting the *I-V* curves to a polynomial. These trials showed 6–8th order polynomials to give roughly equivalent results in most cases, with the higher orders giving consistently better fittings overall. An 8th order polynomial was adopted subsequently as the standard, unless otherwise noted.

Fitting *dI-V* curves to an explicit kinetic model for the pump was done manually, as detailed in the Results.

Chemicals and Solutions

Sodium cyanide and SHAM were from Sigma Chemical Co. (St. Louis, MO), and were prepared as stock solutions at concentrations of 1 and 0.4 M (in ethanol), respectively. HEPES was also from Sigma. Otherwise, all chemicals were Analytical Grade from BDH (Poole, Dorset, UK).

Where appropriate, results are reported ± SE of (*n*) observations.

Results

ATP, Cyanide and Guard Cell Potentials

Evidence, in vivo, for primary charge transport in higher plant cells (Poole, 1978; Cheeseman et al., 1980), algae (Spanswick, 1981; Beilby, 1984; Takeuchi et al., 1985) and fungi (Slayman, 1965; Gradmann et al., 1978; Sanders & Slayman, 1982; Blatt, Rodriguez-Navarro & Slayman, 1987) has generally relied on the effects of inhibitors of cellular metabolism, such as cyanide and azide, as well as compounds, including diethylstilbesterol (DES), dicy-

Table 1. *Vicia* guard cell potential (V_m) and conductance (G_m) response to NaCN plus SHAM[a]

	Control	+NaCN/SHAM
V_m/mV	−176 ± 9	−98 ± 13
G_m/S m^{-2}	1.79 ± 0.29	1.13 ± 0.25

[a] Measurements taken before, and 60–90 sec following inhibitor additions. Values for V_m (n = 13, 9 cells) are from the chart records; values for G_m (n = 8, 5 cells) were calculated from voltage-clamp records taken approx. ±30 mV from V_m. No consistent variation in response was observed between 0.3 and 1.0 mM NaCN, and the data have been pooled accordingly. Conductances were somewhat higher than previously reported (Blatt, 1987*a*), but the difference is not significant ($P > 0.05$).

clohexylcarbodiimide (DCCD) and vanadate, which are thought to attack specifically selected, membrane-bound ATPases. The fact that previous attempts failed to elicit electrical responses to cyanide from guard cells (Saftner & Raschke, 1981) can be ascribed now to the deleterious effects of microelectrode salt leakage (Blatt, 1987*a*).

Figure 2 shows the records from four cells exposed to 0.3 and 1.0 mM NaCN plus 0.4 mM SHAM (*see also* Table 1). In all cases, inhibitor treatment resulted in rapid, positive-going ("depolarizing") changes in the recorded potential. Cell potentials shifted by +45 to +103 mV in the first minute of exposure, and usually, a new stable potential was achieved within 60–90 sec (Fig. 2*B–D*). On two occasions (*cf.* Fig. 2*A*), cell potentials were observed to drift over the subsequent 5–10 min, and in one of three trials with 1 mM NaCN alone (without SHAM, *not shown*), the potential recovered approx. 70% of its initial value over 4 min, even in the presence of the inhibitor. In all but one trial, V_m recovered over 4–10 min on washing out cyanide.

Despite the variability in response over several minutes, the early changes in cell potentials showed very similar time courses. Attempts at fitting these changes, after digitizing the potentials from six cells at 2-sec intervals (0–10 sec in NaCN plus SHAM) and then 10-sec intervals (10–90 or 120 sec in NaCN plus SHAM), gave excellent results with a single falling exponential (*see* Methods). Fittings for the traces in Fig. 2, and for the additional two trials subjected to the analysis, indicated a mean response half-time of 10.3 ± 1.7 sec (n = 6; range, 5.1–14.3 sec; $s^2 \leq 1.29 \times 10^{-3}$).

A very similar time course was observed in guard cell ATP pool size during metabolic blockade. The ATP contents of *Vicia* guard cells were followed with time in 1.0 mM NaCN and 0.4 mM SHAM in three separate experiments, and the results are summarized in Fig. 3, fitted together to a

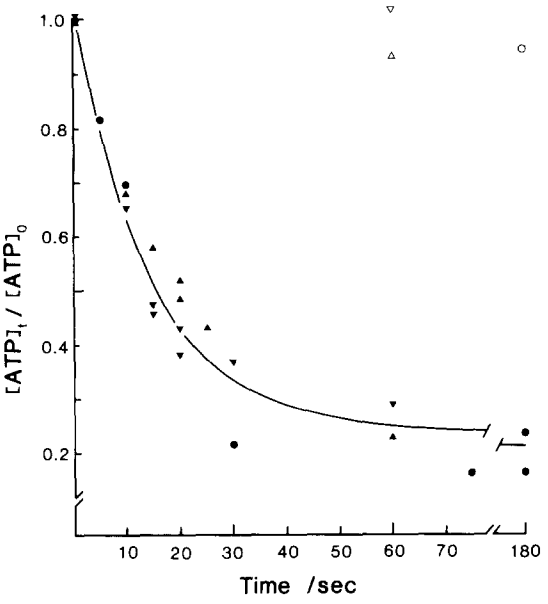

Fig. 3. ATP pool depletion in 1.0 mM NaCN and 0.4 SHAM. Symbols refer to three separate experiments. Data were normalized to the initial (control) values in each experiment and fitted to a single falling exponential (*see* Materials and Methods) to give a depletion halftime of 11.7 sec and final ATP content ($t = \infty$) of 22% ($s = 8.9 \times 10^{-2}$). Open symbols are exposures to 0.4 mM SHAM alone

single falling exponential. The cellular ATP contents of the controls (-NaCN, -SHAM) in the three experiments were 1.85, 1.21 and 0.89 mM, expressed on a cytoplasmic volume basis (stomatal densities, 38–43 mm^{-2}; assumed guard cell cytoplasmic volume, 1.5 pl). Cellular ATP pools declined within 1–3 min to 16–36% of the controls (-NaCN, -SHAM) in NaCN and SHAM, but not in SHAM alone. These figures parallel analogous measurements from fungal and plant cells (*cf.* Slayman, Long & Lu, 1973; Felle, 1981; Roberts, Wemmer & Jardetsky, 1984; Roberts et al., 1985), including *Vicia* guard cell protoplasts (Shimazaki et al., 1983).

It was of some interest that variations in ATP content, while not large, nonetheless were well in excess of the differences in assay yields (*see* Methods). These variations might be ascribed to the physiologic status of the individual plants. Fitting the data from each experiment (plant) separately, however, gave results close to those obtained with the pooled data (*see* legend to Fig. 3). Means for the ATP-pool depletion halftime and for the final (extrapolated) ATP content were 10.8 ± 1.9 sec and 23 ± 7% of the controls, respectively.

Current-Voltage Characteristics

A simple interpretation of the cyanide-induced changes in cell potentials and ATP content is that of

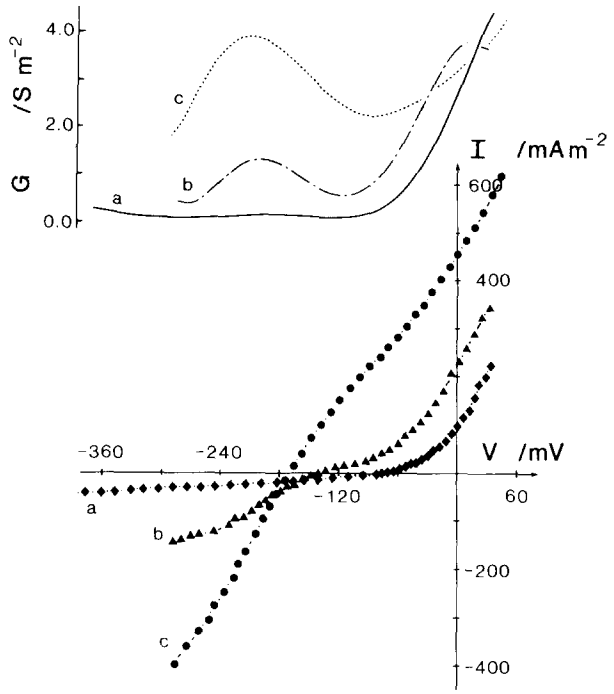

Fig. 4. Steady-state *I-V* and *G-V* characteristics of *Vicia* guard cells. Curves are different cells in three separate experiments, but under similar experimental conditions. Current-voltage curve *a* (V_m, −83 mV) is from a cell previously impaled with a microelectrode and essentially describes a Goldman-like diffusion regime. Curves *b* (V_m, −141 mV) and *c* (V_m, −172 mV) show additional sigmoidicity negative to −120 mV. With the exception of curve *a*, fitted with a 6th order polynomial, curves were fitted to an 8th order polynomial in this, and subsequent figures. Conductance-voltage relations were obtained by differentiating the polynomials

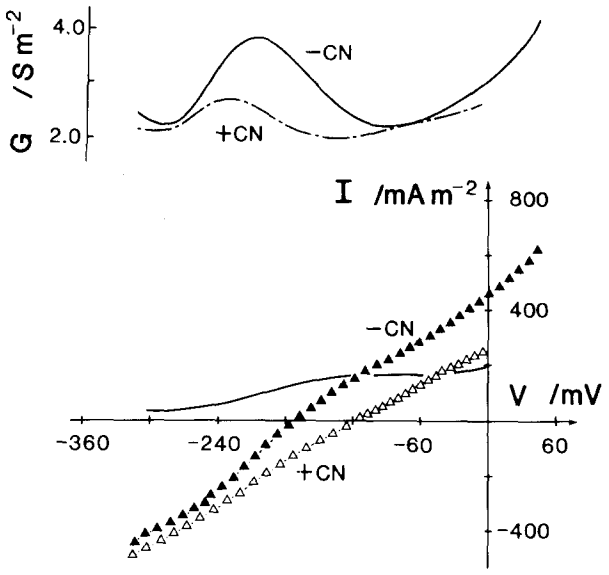

Fig. 5. Steady-state *I-V* and *G-V* characteristics before (▲) and after (△) adding 1.0 mM NaCN and 0.4 mM SHAM (±CN). Corresponding voltage trace *B* in Fig. 2. Voltage limits were altered between scans when large inward and outward currents were recorded near −320 and +60 mV without the inhibitors. The conductance maximum near −220 mV was reduced and downshifted (left) −34 mV in the presence of cyanide. The solid line in the *I-V* plot is the difference current profile obtained by subtraction of 8th order polynomials fitted to the *I-V* data, ▲–△

an "electrogenic" component to the guard cell potential, closely tied to metabolic ATP production. Membrane potentials negative to −210 mV in 0.1 mM K_o^+ are well negative of even the K^+ diffusion potential likely prevailing (*see* Fig. 2*D*; also Blatt, 1987*a*); but the thermodynamic argument provides little or no insight into modes of pump regulation or of its interaction with parallel transport processes in the membrane. A clear knowledge of the voltage-dependence for transport is essential.

Figure 4 shows the current-voltage (*I-V*) and the corresponding conductance-voltage (*G-V*) profiles for three cells impaled in separate experiments. Currents in this, and all subsequent figures (unless otherwise noted) were sampled during the final 20 msec of each 100-msec clamp step, when the membrane current would have reached a quasi-steady state (*see* Appendix); currents were related to membrane surface area assuming an "electrically spherical" cell geometry (*see* Blatt, 1987*a*, also Methods and Appendix for details). The curves reveal a remarkable degree of detail, in direct contrast with the primarily linear *I-V* relations obtained from other higher plant cells in situ (Felle, 1982) or, to date, in suspension (Köhler & Bentrup, 1983). An explanation for this distinction lies, in part, with the unique (electrical) isolation of guard cells within the epidermic and is discussed in the Appendix.

Guard cell *I-V* relations were typically convex to the voltage axis at potentials approaching and positive of 0 mV. Curve *a* was gathered from a cell which had been impaled previously, and from which the first electrode had been withdrawn; the curve is essentially linear, gently sloping to more negative potentials from V_m (−83 mV in this case), and resembles an outwardly-rectifying Goldman diffusion regime (Hodgkin & Katz, 1949). With less harsh handling, guard cells exhibited *I-V* relations, additionally, with varying degrees of concavity to the voltage axis at potentials negative to approx. −100 mV and a conductance maximum (G_{max}) near −220 mV. Comparing curves *b* and *c*—and contrasting curve *a*—to similar voltage clamp data from *Chara* (Beilby, 1984) and *Neurospora* (*cf.* Slayman & Sanders, 1985; Blatt & Slayman, 1987) intimates activity of the pump in the sigmoid curvature about V_m and in the distinctive G_{max}.

The *I-V* profiles from one guard cell, voltage

clamped first in the absence and then in the presence of NaCN plus SHAM, are shown in Fig. 5. The corresponding voltage trace is *B* in Fig. 2 and the *I-V* scans were taken at the times indicated by the carats above the trace. Again, in the absence of the inhibitors, voltage clamping revealed a profile roughly sigmoid in shape about V_m, and a characteristic G_{max} near −220 mV. At V_m (I_m = 0, *V*-axis intercept) the conductance was 3.30 S m^{-2}, and the short-circuit current (I_{ssc}, *I*-axis intercept, V = 0) was close to 450 mA m^{-2}.

Adding NaCN plus SHAM (but not SHAM alone, *data not shown*) eliminated the sigmoidicity in the *I-V* characteristic, reducing G_{max} against the background conductance. Along with a +60 mV shift in V_m, G_m fell to 2.12 S m^{-2} and I_{ssc} was reduced by 44% to 255 mA m^{-2} (*see also* Table 1). Note, too, that G_{max} was shifted to the left (-)34 mV along the voltage axis. Qualitatively similar results were obtained in an additional four cells and seven trials with cyanide plus SHAM (*see* Table 1, also Fig. 9).

Difference-Current-Voltage Characteristics

Steady-state currents, measured as a function of the (clamped) membrane potential, reflect the sum of *all* charge-carrying pathways in the membrane; the problem, then, is to dissect out those currents specific to the pump. One common empirical approach to extracting the voltage-dependent kinetic (*I-V*) characteristic for a single transport process is to *subtract* the currents across the accessible voltage spectrum to yield a *difference I-V* (*dI-V*) relation. This operation makes the explicit assumption that changes in the whole membrane *I-V* relation, effected by experimental manipulation, are confined to the transport process in question. In the present context, then, the pump *dI-V* characteristic is derived at every voltage as

$$\Delta i_P = i^{-CN} - i^{+CN} = i_P^{-CN} - i_P^{+CN} \quad (2)$$

where the superscripts denote the condition of cyanide exposure, the subscripts refer to the pump, and the nonsubscripted currents are experimental values.

The *dI-V* curve derived from the parent *I-V* data is included in Fig. 5 (solid line). Again, very similar curves were obtained from the other four cells, and Fig. 6 illustrates the range of *dI-V* curves found. Difference current profiles showed a region between approx. −300 and −100 mV over which the pump difference current was voltage dependent. Little or no sensitivity of the current to voltage was

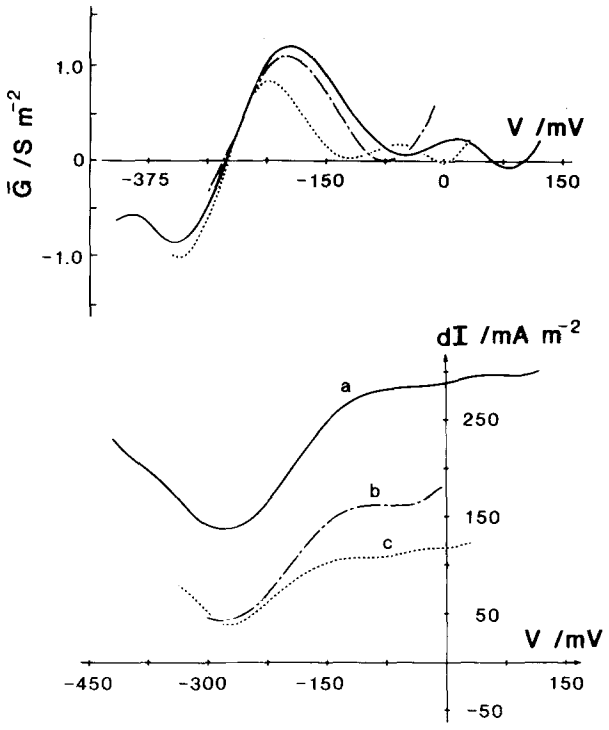

Fig. 6. Difference-current-voltage relations from three cells. The currents in curve *a* were exceptionally large (*see also* Fig. 9 and Table 2 for relevant *I-V* data and fitting). Currents, near 0 mV, between 100 and 200 mA m^{-2} were typical (curves *b* and *c*). Corresponding $\bar{G}$–*V* relations showed a prominent inflection near −300 mV

observed for membrane potentials positive of approx. −100 mV.

A singular feature of these *dI-V* relations was their general failure to *cross* the voltage axis. On one occasion only (*not shown*) was there any indication of a zero-current (crossover) potential which might have been construed as an equilibrium potential; but in this instance, the crossover point was so close to the limit of the voltage scan as to render its significance doubtful. By contrast, in two of the data sets (*see* Fig. 6), it was possible to extend the voltage range sufficiently to show that the difference currents actually *increased* at progressively more negative potentials beyond −300 mV. Beilby (1984) observed a similar bias in subtracting currents for the *Chara* H^+ pump.

Why should the pump *dI-V* curves fail to cross the voltage axis, even at membrane potentials approaching −450 mV? An unambiguous answer lies in the operation of subtracting currents itself (Blatt, 1986), rather than any ill-defined changes in secondary membrane characteristics. The reasons behind this property of *dI-V* relations are not intuitively obvious and deserve a closer look. While current subtraction cannot yield transport equilibrium

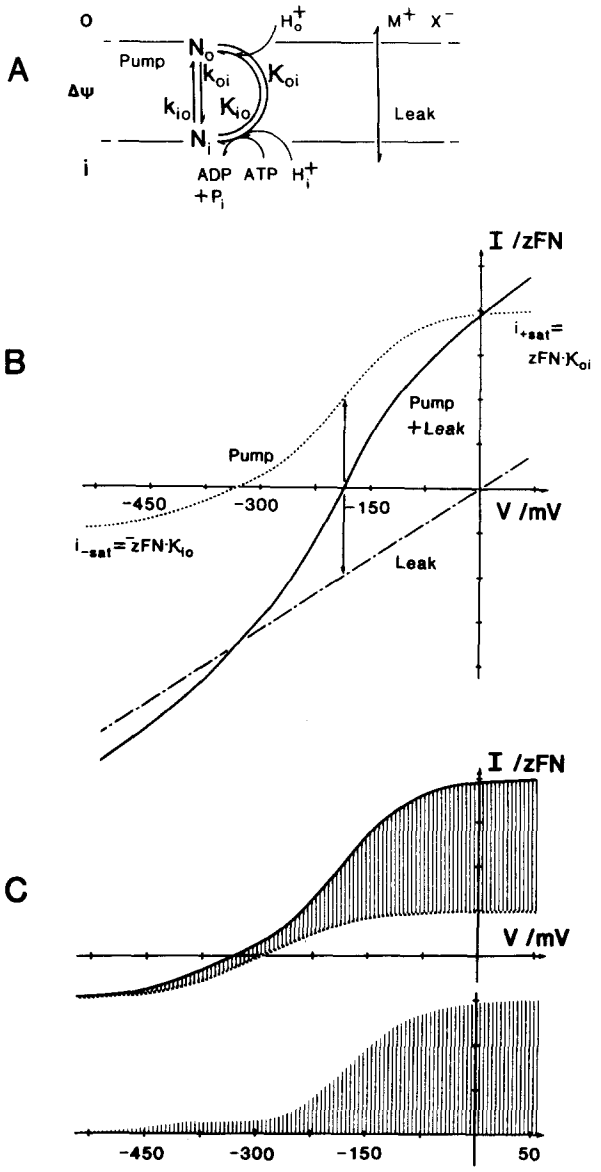

Fig. 7. Model ("reduced," 2-state) pump and ohmic leak. (*A*) Schematic of pump and leak in the membrane. Pump drawn assuming a neutral carrier in the unloaded state. Voltage sensitivity is restricted to the reaction constants k^o_{io} and k^o_{oi}. Binding/debinding and (unloaded) carrier recycling steps are subsumed in the constants κ_{io} and κ_{oi}. Ionic characteristics of the leak are left unspecified. (*B*) Hypothetical whole cell *I-V* curve and its component pump and leak curves, as derived from the model. The reaction constants κ_{io} and κ_{oi} determine the relative values of the voltage-saturated currents, i_{-sat} and i_{+sat}. Pump and leak equilibrium potentials (E_P, E_L) are defined by the respective zero-current potentials; at the free-running membrane potential (V_m), pump and leak currents are equal and opposite (arrows). (*C*) Difference-current-voltage curve derived for a hypothetical ion pump. Solid curve is the pump curve in *B*. Experimental manoeuver to inhibit the pump affects κ_{oi} only and reduces it (dotted curve). Difference currents are obtained by subtracting the dotted curve from the solid curve (shading). The operation eliminates the (unaffected) leak in the *dI-V* curve, so leak currents are not shown for the *I-V* curves

(zero-current) potentials directly, *dI-V* characteristics do inherit a great deal of kinetic information from their parent *I-V* curves. For the guard cells, the *dI-V* relations readily accommodate a charge stoichiometry of one, but not two, positive charges moved out of the cells per transport cycle.

Kinetic Analysis of the Pump

Three salient features of charge transporting processes are (i) the equilibrium potential (E_{trans}), which defines the thermodynamic limit for net charge movement in either direction across the membrane ($i_{net} = 0$); (ii) current saturation in the steady state at voltages well away from E_{trans}; and (iii) a voltage span about E_{trans} over which transport current (velocity) is voltage dependent and increases with (and of the same sign as) the prevailing voltage difference from E_{trans}. Kinetic models, which incorporate a voltage-dependent factor into one or more partial reaction steps, impart to the model these three characteristic properties.

For purposes of *I-V* analysis, conventional carrier models comprising a single transport loop with one voltage-dependent transition can be 'reduced' to a minimum of two carrier states and four empirical reaction constants (Hansen et al., 1981), as shown in Fig. 7*A*. Two reaction constants incorporate explicitly a voltage-sensitive component and describe transmembrane charge transit (k_{io}, k_{oi}); the remaining constants (κ_{io}, κ_{oi}) represent carrier movement through the electrically transparent limb of the reaction cycle, including ligand binding/debinding steps on either side of the membrane. In the steady state, the net current through the transporter (pump) is defined by the equation

$$i_P = zFN \cdot \frac{k_{io}\kappa_{oi} - k_{oi}\kappa_{io}}{k_{io} + k_{oi} + \kappa_{io} + \kappa_{oi}} \qquad (3)$$

where $k_{io} = k^o_{io}e^{zu/2}$, $k_{oi} = k^o_{oi}e^{-zu/2}$, and z is the net charge transported with each carrier cycle. The specific reaction constants k^o_{io} and k^o_{oi} are voltage independent and their values are defined at zero membrane potential ($V = 0$); the reduced voltage $u = FV/RT$, where F, R and T have their usual meaning, and (as a first approximation) the factor 2 places the potential (Eyring) barrier symmetrically within the membrane (Läuger & Stark, 1970).

Weightings of the reaction constants can be found for which *I-V* profiles generated using Eq. (3) resemble guard cell *I-V* characteristics (Fig. 7*B*), provided that the modelled curve is summed with a simple, ohmic leak taken to represent all other charge-carrying processes in the membrane (*see*

Sanders et al., 1981; Gradmann, Hansen & Slayman, 1982). These curves illustrate, also, the consequence of subtracting currents.

For the model shown, the forward, voltage-dependent constant κ_{oi} subsumes ATP- and ion-(transportee-) binding steps on the inside of the membrane. So, in the first instance, depleting the cell of ATP by metabolic poisoning will decrease κ_{oi} by reducing the rate of this ATP-binding step. The consequence for the modelled pump *I-V* characteristic is to decrease the value of the voltage-saturated current at extreme positive potentials, and to shift the reversal potential to the right along the voltage axis (Fig. 7*C*). Now it can be seen that subtracting the two *I-V* curves, *just as would be done to eliminate the background of unaffected transport processes*, fails to reveal the equilibrium potential for transport simply because the experimental maneuver affects the equilibrium potential itself (Blatt, 1986).

The situation is likely to be complicated slightly for metabolic poisons such as cyanide. Depleting ATP pools leads to complementary increases in cellular ADP and inorganic phosphate (P_i) content (Chapman, Johnson & Kootsey, 1983; Roberts et al., 1984, 1985). Binding of these ligands affects reverse operation of the transport cycle and, analogously, can be expected to increase the magnitude of κ_{io} and of the voltage-saturated current at extreme negative potentials.

For analysis of the voltage clamp data (±cyanide) from the guard cells, fittings were carried out manually using Eqs. (2) and (3). Two starting assumptions were made: (i) as before, the leak was assumed to be unaffected by cyanide treatment during the time between *I-V* measurements, ±cyanide; and (ii), forward operation of the pump was presumed to be reduced, but not blocked by cyanide treatment. Estimates for the forward, voltage-independent constant κ_{oi} were constrained to a 4:1 (−cyanide:+cyanide) relationship consistent with the data in Fig. 3 and, initially, κ_{io} was allowed to follow κ_{oi} in inverse proportion.

The first assumption meant that fitting could be carried out to the *difference* current (*dI-V*) relation, *independent* of ad hoc assignments for the ensemble leak. The second point was the simplest in which to view, quantitatively, the effect of ATP withdrawal on the pump (*cf.* Gradmann et al., 1978, 1982; Slayman & Sanders, 1985). [This second assumption also implied that the ensemble leak reversal potential, E_L, should be found at voltages positive of V_m (+CN), because limited operation of the pump requires current return via the leak. However, no explicit restriction was applied in solving for E_L (*see below*).] Finally, additional guidelines for reaction constant ratios were drawn from the shape of the experimental *dI-V* curves [*see* Eqs. (15)–(19) and (26), the Table, and accompanying discussion in Blatt (1986)]. A starting value of 10 for the ratio $(\kappa_{io} + \kappa_{oi})/(k^o_{io}k^o_{oi})^{1/2}$ was suggested by *dI-V* conductance inflections and peak-to-peak (positive-negative) spread (*see* Figs. 6 and 9). Conductance inflections close to −300 mV (*cf.* Fig. 6) also indicated a value near 10^{-5} for the ratio k^o_{oi}/k^o_{io}.

Fitting the *dI-V* data, thus, reduced to a three-step procedure and is illustrated in Fig. 8 for the data of Fig. 5. Quantitatively similar fittings (*cf.* Fig. 9) were obtained in analyses of data sets from the other four cells, and Table 2 summarizes these results and related parameters. First, values for κ_{oi} were chosen to give a 4:1 ratio (−cyanide:+cyanide) and satisfy, for voltages positive to approx. −100 mV where the difference current appeared to saturate,

$$\Delta i_P = zFN \cdot (\kappa_{oi}^{-CN} - \kappa_{oi}^{+CN}) \tag{4}$$

by analogy with Eq. (20) of Blatt (1986). Difference currents were calculated, across the voltage span of the data, using the reaction constant estimates and Eqs. (2) and (3). Fitted and experimental *dI-V* curves were inspected, and values for the constants were adjusted accordingly. Because clues to the relative magnitudes of κ_{oi}, k^o_{io} and k^o_{oi}, primarily, could be expected in the shape of the *dI-V* profile positive to approx. −300 mV, emphasis was placed on matching fitted and experimental curves over this voltage range.

Second, values for the leak conductance (G_L) and equilibrium potential (E_L) were assigned. These estimates were taken from the predicted pump currents, which at V_m (±cyanide) must just balance current passage through the leak ($i_m = 0$), and from the intersections (at a common voltage, ±cyanide) of the experimental and fitted pump *I-V* curves, which define E_L ($i_L = 0$). In practice, a straight line could be drawn through all three points (*see* Fig. 8*B,C*).

Finally, this empirical characteristic for the leak was extended across the accessible voltage spectrum, and the *I-V* relations (used to construct fitted *dI-V* curves) were translated to the experimental *I-V* data. Formally, the translation was accomplished according to the relations

$$i_m = i_P + i_L \tag{5a}$$

and

$$i_L = G_L(V - E_L) \tag{5b}$$

Table 2. Pump characteristics for *Vicia* guard cells[a]

Data set in	Figs. 9	Figs. 5, 8	Summary
k^o_{io}	4.2×10^3	2.0×10^3	
k^o_{oi}	9.0×10^{-2}	4.0×10^{-2}	
κ_{io}	2 (27)	1 (5)	
κ_{oi}	40 (10)	24 (6)	
k^o_{oi}/k^o_{io}	2.1×10^{-5}	2.0×10^{-5}	$1.7 \pm 0.2 \times 10^{-5}$
$\frac{(\kappa_{io} + \kappa_{oi})}{(k^o_{io}k^o_{oi})^{1/2}}$	2.2	2.8	2.2 ± 0.3
E_P/mV	−352	−359	-358 ± 4
i_{+sat}/mA m^{-2}	400	240	220 ± 50
i_{Vm}/mA m^{-2}	206	164	160 ± 10
G_P/S m^{-2}	1.3	0.9	0.8 ± 0.1
G_L/S m^{-2}	0.9	2.1	1.3 ± 0.3
E_L/mV	−14	−88	-66 ± 13

[a] Reaction constants and related parameters for the pump and leak derived from fittings shown in Figs. 8 and 9. Reaction constants listed are implicit products of the corresponding empirical rate constants and the, as yet unknown, pump density N (mol m^{-2}, for the present assigned a value of unity). Values in parentheses are in the presence of cyanide. Quantitatively similar sets of reaction constants were obtained in the three other analyses carried out; fitted pump and leak equilibrium potentials (E_P, E_L) and conductances (G_P, G_L), and pump currents at positive saturating voltages (i_{+sat}) and at the prevailing membrane potential (i_{Vm}) are summarized for all five data sets. Note the energetic asymmetry in the pump cycle is predominant in the membrane charge-transit step (k^o_{oi}/k^o_{io}) and strongly favors forward operation of the pump (*compare* e.g. Slayman & Sanders, 1985).

where i_m, i_P and i_L are the membrane, pump and leak currents at every (clamped) membrane potential V, and i_P is given by Eq. (3). For extended *I-V* data, the reaction constant κ_{io} (±cyanide) was refined secondarily [κ_{oi} (±cyanide) and the ratio k^o_{oi}/k^o_{io} constant], with the common ohmic leak, to the difference currents and parent *I-V* characteristics near the negative voltage extreme.

Visually satisfactory fittings to the *dI-V*, and even to the *I-V* data (*but see* Fig. 9, inset) were obtained surprisingly quickly by this means. Gratifying, too, was the fact that the predicted G_{max} for the pump in cyanide was downshifted along the voltage axis (*compare* Figs. 8 and 5). Nonetheless, *I-V* scans generally terminated at voltages near −350 mV, or well before the pump current could be expected to achieve voltage independence at the negative extreme. So, values for κ_{io} remain uncertain, a fact which could account for quantitative discrepancies in G_{max} positions between fitted and experimental *G-V* curves. [Deviations of the fitted *I-V* curves from the guard cell data (*see* Fig. 9, inset) may be related, also, to the linear leak assumed (*see* Discussion)]. The reaction constant-scalar product $N \cdot \kappa_{oi}$ (and, hence, G_L and E_L) as well as the ratio k^o_{oi}/k^o_{io} were derived independently of κ_{io}, and these estimates are unaffected. Otherwise, values of the individual reaction constants and the related parameter E_P quoted in Table 2 should be treated as preliminary. Combinations of reaction constants could be found, after minor adjustments to κ_{io}, k^o_{oi} and k^o_{io}, which gave equivalent fittings to the *I-V* and *dI-V* data, and yielded values for E_P as large as (−)480 mV in the respiring cells. Physiological interpretations for the leak parameters are taken up in the Discussion.

I carried out a systematic review of alternative preconditions for charge : carrier-cycle stoichiometry using three data sets, including the data of Figs. 5 and 6. Attempts to match the experimental *dI-V* curves using integral charge stoichiometries higher than 1(+) : carrier cycle [equivalent to 1(H^+ transported) : 1(ATP hydrolyzed)] were wholly unsuccessful (results *not shown*). As expected (Blatt, 1986), the principal restriction in this instance was the shallow conductance of the *dI-V* profile about the conductance inflection.

Discussion

Cyanide and the Pump

The choice of agents for blocking primary ion pumping in plant cells and fungi remains largely unsatisfactory. Cyanide (Gradmann et al., 1978), DES (Beilby, 1984), DCCD (Kishimoto et al., 1984) and vanadate (Bowman & Slayman, 1979; Blatt & Slay-

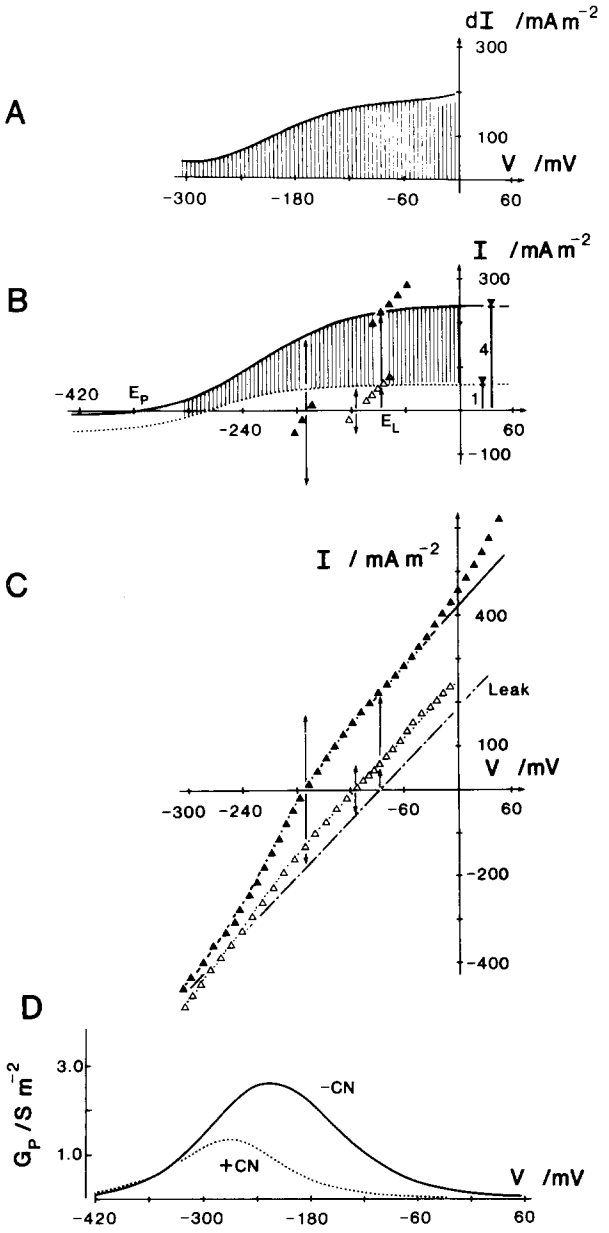

Fig. 8. Fitting the pump-leak model to guard cell *I-V* and *dI-V* relations. Data of Fig. 5. (*A*) Experimental (solid line) and fitted (shaded) difference currents. The small discrepancy near 0 mV might indicate an effect of the inhibitors on an outwardly-rectifying leak (*see* Discussion). (*B*) Modelled pump *I-V* curves yielding the difference currents (shaded) in *A*. The 4 : 1 constraint on i_{+sat} (±cyanide) is indicated on the right. Pump currents (↑) at V_m (±cyanide) are mirrored at the voltage axis to obtain the leak currents at these potentials (↓). A third point on the leak (E_L, i_L = 0) is defined by the common voltage at which modelled pump and experimental *I-V* curves intersect. (*C*) Experimental *I-V* data (▲, -cyanide; △, +cyanide) fitted to the modelled curves in *B* summed with the leak. Once the leak profile is determined (arrows, as above), total (fitted) membrane current can be found at every voltage by Eq. (5). (*D*) Model *G-V* profiles for the curves in *B*. Note the reduced and downshifted G_{max} "in" cyanide (−37 mV, *compare* Fig. 5). Final parameter values listed in Table 2

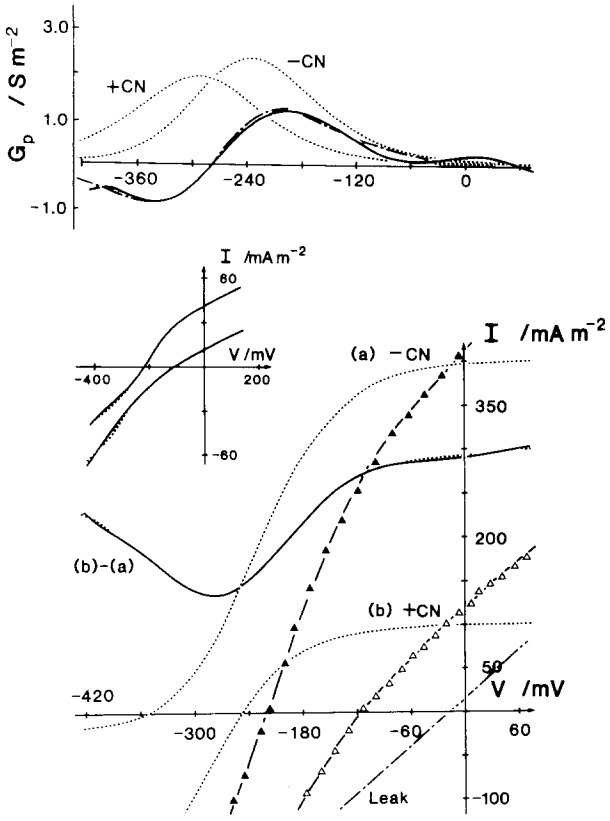

Fig. 9. Extended guard cell *I-V* and *dI-V* relations fitted to the pump-leak model. Experimental *dI-V* curve (solid line, 8th order difference polynomial) overlies most of the fitted curve (dotted line). Modelled pump *I-V* curves (*a*, *b*) were added to the leak (——) to give the fittings to the data points (▲, −CN; △, +CN). Modelled pump conductance- (G_P, – – – –) and modelled (——) and experimental (——) difference conductance-voltage curves are shown above. *Inset*: marked deviations of the fitted curves (dotted lines) from the experimental *I-V* curves (solid lines). Final parameter values listed in Table 2

man, 1986; *see also* Sze, 1985) have been used, with varying degrees of success, to identify ATP-dependent ion transport and H^+ pumping. The precedents notwithstanding, specificities of all of these agents, at least in vivo, is likely to be poor. DCCD blocks the mitochondrial and chloroplast F_0F_1 and CF_0CF_1 ATPases as well as the E_1-E_2-type H^+-ATPase of plant plasma membranes (Goffeau & Slayman, 1981; Sze, 1985). DES is known to affect current passage through the *Chara* "K^+ state" K^+ channel as well as affecting the background membrane conductance (Beilby, 1984, 1986). Likewise, vanadate can be expected to attack a range of enzymatic processes, including protein kinases and phosphatases of secondary messenger systems (Swarup et al., 1982; Tracey & Gresser, 1986), for which phosphate transfer passes through a tri-

gonalbipyramidal configuration. Vanadate is known to block the coupled transport of K^+ with H^+ in *Neurospora* independent of its effect on the H^+-ATPase (Blatt & Slayman, 1986; Blatt et al., 1987).

Because of the multiple effects likely with each of these compounds, demonstrating the presence in vivo of a primary, ATP-consuming pump—let alone one which carries protons—is necessarily indirect. My choice of cyanide was founded not on a basis of selectivity, but rather on the assumption that a fall in the cellular ATP pool should be detected first in charge movements coupled directly to the hydrolysis of ATP. As was observed, early changes in V_m closely followed the time course for ATP depletion. Likewise, cyanide-induced changes in the *I-V* and *G-V* relations are most easily understood as a direct result of a drop in cellular energy charge and the consequent fall in current output by the pump.

Nonetheless, much slower changes in guard cell potentials (*see* Fig. 2*A*)—with halftimes on the order of minutes rather than seconds—underscore the hazards of the approach. These changes continued well past the time when cellular ATP pools reached a new steady state; they intimate secondary effects of cyanide treatment possibly only indirectly related to metabolic blockade (*cf.* Sanders & Slayman, 1982). Clearly, indiscriminant use of the inhibitors over many minutes is likely to distort comparisons, in particular, between membrane potential and ATP content (*cf.* Mercier & Poole, 1980; also discussion by Lew & Spanswick, 1984). This same concern must apply also to *I-V* analyses of primary transport (*see* Blatt, 1986, for discussion) and, *vide infra*, to correlative studies of net H^+ flux with vanadate and DES (*cf.* Gepstein et al., 1982; Shimazaki et al., 1986).

Charge Stoichiometry of the Pump

Support for the idea that a single charge is transported for each ATP hydrolyzed may be derived independently of specific models for the pump. The free energy available from the hydrolysis of ATP can be compared directly with the electrical potential and, assuming the ion transported in the proton, the pH gradient generated across the membrane. The membrane potential which just balances the driving force of the pump

$$E_P = \frac{RT}{zF}\left[\ln K_{ATP} + \ln \frac{[ATP]_i}{[ADP]_i[P_i]_i} + z \ln \frac{[H^+]_i}{[H^+]_o}\right] \quad (6)$$

where K_{ATP} is the equilibrium constant for ATP hydrolysis and z is the number of charges carried per transport cycle. In the absence of an appreciable pH gradient across the membrane, the free energy for ATP hydrolysis near neutral pH values (Walker & Smith, 1975; Gradmann et al., 1978) indicates a stalling potential close to (−)500 mV for a $1(H^+):1(ATP)$ pump. A $2(H^+):1(ATP)$ pump would stall near (−)250 mV, either positive or uncomfortably close to membrane potentials actually recorded from guard cells (*see* Fig. 2; also Blatt, 1987*a*).

In fact, fitting the *dI-V* curves with a unitary charge stoichiometry indicated, for the respiring cells, pump equilibrium potentials between −350 and −375 mV, or well in excess of the (−)250 mV mark. These fittings required only that K_{io} rise as

$$\Delta\kappa_{io}/\kappa_{io}^{+CN} = (\Delta\kappa_{oi}/\kappa_{oi}^{-CN})^{-m} \quad (7)$$

where the superscripts denote the reaction constants in the presence and absence of cyanide, and $m < 2$. Roberts et al. (1985) showed recently that ADP levels are normally below the limit for detection by ^{31}P-NMR in respiring corn root segments, but are easily measured on adding cyanide plus SHAM. They estimated the rise in ADP conservatively at 25-fold. Given such a dramatic change in the [ATP]/[ADP] ratio of the guard cells, the relationship in Eq. (7) could be accommodated explicitly by a corresponding rise in the product $[ADP][P_i]$, even against a background of millimolar internal P_i (Walker & Smith, 1975; Roberts et al., 1984).

Implications for Guard Cell Physiology

The merit of any model ultimately rests in its ability to focus experimental research by anticipating the outcome. Two aspects of the *dI-V* analyses bear directly on guard cell behavior. The first point relates to the magnitude of the current generated by the pump, and the second deals with the implications of its voltage dependence.

At the prevailing membrane potential fitted pump currents for the respiring cells were in the range of 100–200 mA m^{-2} (mean, 160 ± 10 mA m^{-2}; *see* Table 2). [A crude estimate of the pump current, taken directly from the *dI-V* curves, gives a range of 60–180 mA m^{-2}. The approach is treacherous (Blatt, 1986), but yields similar results in this instance.] Corresponding H^+-pump currents of carbon-replete *Neurospora* generally fall between 200 and 300 mA m^{-2} (*cf.* Slayman & Sanders, 1985), and for *Chara* the currents scatter about a value of 100 mA m^{-2} (Beilby, 1984).

Comparing these currents with recent studies of *Vicia* guard cell protoplasts, however, shows up inconsistencies. There is one report of ATP-dependent ion pumping; Assmann et al. (1985) observed blue-light-induced currents approaching 10 mA m^{-2}, or roughly 20-fold lower than I found for the intact guard cells. Net proton extrusion rates from the protoplasts (2–6 pmol cm^{-2} sec^{-1}, Shimazaki et al., 1986) and from "isolated" but intact guard cells in epidermal strips (3–10 pmol $cm^{-2}sec^{-1}$, Gepstein et al., 1982, calculated according to MacRobbie, 1987) are close to this mark as well (1 mA $m^{-2} \simeq 1$ peq $cm^{-2}sec^{-1}$). Finally, respiratory and photosynthetic rates (Shimazaki et al., 1983) indicate that 1–2 pmol of ATP turn over per hour in a single protoplast. From the estimated pump current alone, intact guard cells can be expected to consume 5–15 pmol ATP $cell^{-1}hr^{-1}$ while pumping an equivalent number of protons.

With reference to the chemical flux (external pH) measurements, it is essential to recognize that *net* H^+ extrusion requires, in the sum, equivalent movements of other ions to balance charge; it will fall short of the true H^+ pump current in direct proportion with the extent to which electroneutrality is achieved by H^+ *recycling*, for example via H^+-coupled transport. So, it is hardly surprising that net H^+ efflux is balanced by K^+ uptake in guard cells under some conditions (Raschke & Humble, 1973). An unambiguous explanation for the discrepancy between the *currents* is wanting.

One concern must lie in the use of protoplasts itself (Clint, 1985), particularly with guard cells as likely candidates for osmotic/turgor regulation. The choice of experimental conditions may contribute to the discord as well. At least for *Chara* (*but see* Fig. 10 for *Vicia* guard cells), exposure to millimolar K^+ concentrations (2-10 mM) appears to shut down the H^+ pump (Beilby, 1985); work with the guard cell protoplasts was carried out in 10–50 mM K^+ salts (Shimazaki et al., 1983, 1986; Assmann et al., 1985). This same point may account, also, for the apparent difference between metabolic rates and the energetic requirements of the pump; the metabolic activity of cells is coupled tightly to demand (*cf.* Roberts et al., 1985), and membrane transport—ultimately powered by the pump—is likely to be a major consumer of ATP. Clearly, there is a need for comparative transport and biochemical studies of the intact cells and protoplasts.

Turning to the voltage dependence of the current, it will be seen that the pump can contribute appreciably to the total membrane conductance, even at free-running potentials well removed from E_P (*compare* G_P and G_L in Table 2). This feature is a characteristic of transport limited by the intrinsic rate of charge movement across the membrane and has two consequences for guard cell behavior.

First, by operating over the voltage-sensitive span of the pump *I-V* curve, changes in E_P achieved by increasing *trans*-ligand concentrations ($[H^+]_o$ for an outwardly-directed H^+ pump) will be translated to the membrane potential and should be accompanied by little, if any, change in G_m. These predictions come about primarily because the pump *I-V* characteristic should shift to the right along the voltage axis with little change in curve shape positive to E_P (*see* Slayman & Sanders, 1985). In fact, acid-going pH_o jumps have been shown to have little effect on G_m, but do shift guard cell potentials to more positive values (Blatt, 1987*a*). Both in sign and magnitude, this behavior is consistent with the notion of an H^+ pump.

The second consequence is that regulating pump activity is likely to be very inefficient as the *sole* mechanism for controlling secondary transport, such as K^+ uptake. Increasing pump activity against a *constant* leak conductance will drive the membrane potential to more negative values until pump and leak currents are again equal and opposite; but because the pump current itself falls off with the (negative) potential, the voltage response, and hence the change in the driving force for K^+ movement ($= V_m - E_K$, for a K^+ channel), will be attenuated. This same argument has been applied to K^+-H^+ cotransport-dependent recovery from acid stress in *Neurospora* (Blatt & Slayman, 1987). [By contrast, decreasing pump activity against a constant leak, as in the experiments described with cyanide, quickly places V_m beyond the voltage-sensitive range of the pump *I-V* characteristic (*see* Figs. 8 and 9). In this case, V_m comes under direct kinetic control by the pump.]

Implications of the Leak for Guard Cell K^+ Relations

For purposes of *I-V* analysis, the leak is defined by the ensemble of all secondary transport processes and diffusion regimes occurring across the membrane; the assignment reveals little about the nature of the individual components or their characteristics. However, two lines of evidence do suggest that the membrane conductance to K^+ did not dominate the leak in these experiments. First, membrane potentials recorded in the absence of cyanide usually were close or positive to E_K which, with 0.1 mM K^+ outside, was probably near −180 to −200 mV. Second, membrane potentials recorded *in* cyanide generally collapsed to values near or positive to −100 mV.

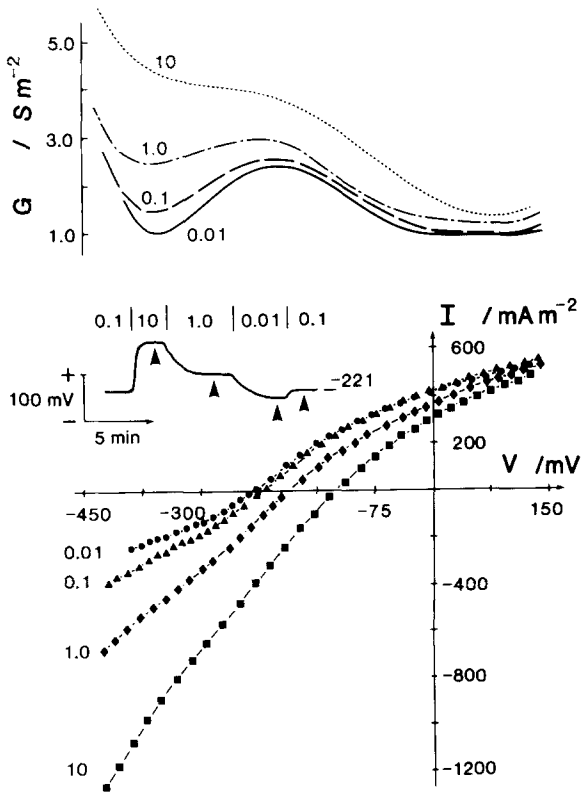

Fig. 10. Inward-rectifying currents in guard cell *I-V* relations. Effect of external KCl (concentrations in mM, indicated on the left). Data from the same cell as Fig. 9. Membrane conductance (G) was affected preferentially toward negative potentials. *Inset*: voltage trace with carats indicating times at which *I-V* scans were run. Pump activity may have been reduced at high KCl concentrations; G_{max} (near −220 mV) appears to fall approx. 2.6-fold at 10 mM KCl against the background conductance, estimated from the tangent to the *G-V* curve between −350 and +50 mV in each case

Now, by reducing the pump current, the free-running membrane potential will relax toward the leak equilibrium potential until pump and leak currents are once again equal. So, a simple interpretation requires that E_L lie *positive* to −100 mV, or well displaced from any reasonable value for E_K. In fact, fitting guard cell *dI-V* and *I-V* curves to Eqs. (2)–(5) indicated values for E_L, which in all cases were situated between −93 and −14 mV (mean, −66 ± 13 mV, *see* Table 2). These estimates do assume that the leak conductance and equilibrium potential were constant during the course of the measurements but, to a first approximation, the requirement appears to hold, as in *Neurospora* (*cf.* Gradmann et al., 1982), for 1–2 min following cyanide additions.

It is worth noting that guard cells apparently lacking in pump activity (*cf.* Fig. 4, curve *a*) showed membrane potentials close to −80 mV and *I-V* relations which were essentially linear to more negative potentials. The rising conductance and currents at more positive potentials are familiar features of plant and fungal cells (*cf.* Gradmann, 1975; Gradmann et al., 1978; Beilby 1984) and may be assigned empirically to a Goldman-like diffusion regime (Blatt & Slayman, 1987). Again, this description says nothing about the nature of the leak, but it provides an insight into discrepancies between experimental data and voltage-saturating models for primary ion transport (*see* Fig. 8); small changes in leak characteristics, too, are likely to be most visible in the rectification (Fig. 8; *see also* Beilby, 1984).

Analyses of membrane potentials and *I-V* relations for *Chara* (Beilby, 1984; Beilby & Blatt, 1986), likewise, argue against a dominant role for K^+ in the passive characteristics of the membrane at low external K^+ concentrations. Nonetheless, the leak cannot be regarded as a single, permanently static or K^+-insensitive fixture. For *Chara*, two (or more?) K^+ channels (Beilby, 1985, 1986; Sokolik & Yurin, 1986) and a Cl^- channel (Tyerman, Findlay & Paterson, 1986) can impart, voltage- and concentration-dependent, inward- and outward-rising currents to the whole membrane *I-V* characteristic. Even a nonlinear (Goldman) model will approximate the true leak *I-V* profile over a limited voltage range only under these conditions.

An analogous situation may exist in guard cells, as well, and bears directly on notions of simple "pump-and-channel" mechanisms for stomatal movements. In recent experiments (Blatt, 1987*b*, and manuscript *in preparation*), I identified an outwardly-rectifying K^+ channel in the rising currents and conductance near 0 mV of the steady-state *I-V* relations. KCl-sensitive, inwardly-rectifying currents have appeared in several recordings, as well. Figure 10 is a good example of this latter phenomenon. Increasing the external KCl concentration over three orders of magnitude (0.01–10 mM) increased the membrane conductance preferentially toward more negative potentials and in a concentration-dependent manner. These features are remarkably similar to those of the K^+ channels Sokolik and Yurin (1986) have reported in *Chara*. If the electrical characteristics hint of possible physiological roles for these currents, what remains uncertain are those factors which dictate their appearance. Nevertheless, it is clear that the variety of pathways available for K^+ movements across the membrane is likely to prove substantially richer than was once thought.

I am grateful to Dr. Keith Johnstone (Botany, Cambridge) for tips on the ATP assays, and to Dr. David Kerridge (Biochemistry, Cambridge) for access to the luminometer. My special thanks to Dr. Mary Helen Goldsmith (Biology, Yale) and to Prof. E.A.C. MacRobbie (Botany, Cambridge) for comments

and suggestions on the manuscript, to Dr. Dale Sanders and Mr. Ian Jennings (Biology, York) for their Marquardt fitting program, and to Dr. Bruce Beilby (Sydney) for his help early on with the programming. This work was supported by a grant from the SERC.

References

Assmann, S., Simoncini, L., Schroeder, J. 1985. Blue light activates electrogenic ion pumping in guard cell protoplasts of *Vicia faba*. *Nature (London)* **318:**285–287

Beilby, M. 1984. Current-voltage characteristics of the proton pump at *Chara* plasmalemma: I. pH dependence. *J. Membrane Biol.* **81:**113–126

Beilby, M. 1985. Potassium channels at *Chara* plasmalemma. *J. Exp. Bot.* **36:**228–239

Beilby, M.J. 1986. Factors controlling the K^+ conductance in *Chara*. *J. Membrane Biol.* **93:**187–193

Beilby, M., Blatt, M.R. 1986. Simultaneous measurements of cytoplasmic K^+ concentration and the plasma membrane electrical parameters in single membrane samples of *Chara corallina*. *Plant Physiol.* **82:**417–422

Blatt, M.R. 1986. Interpretation of steady-state current-voltage curves: Consequences and implications of current subtraction in transport studies. *J. Membrane Biol.* **92:**91–110

Blatt, M.R. 1987*a*. Electrical characteristics of stomatal guard cells: The ionic basis of the membrane potential and the consequence of potassium chloride leakage from microelectrodes. *Planta* **170:**272–287

Blatt, M.R. 1987*b*. Fusicoccin, K^+ channels and stomatal closure. *Plant Physiol.* **83:**145A

Blatt, M.R., Rodriguez-Navarro, A., Slayman, C.L. 1987. Potassium-proton symport in *Neurospora*: Kinetic control by pH and membrane potential. *J. Membrane Biol.* **98:**169–189

Blatt, M.R., Slayman, C.L. 1983. KCl leakage from microelectrodes and its impact on the membrane parameters of a nonexcitable cell. *J. Membrane Biol.* **72:**223–224

Blatt, M.R., Slayman, C.L. 1986. Current-voltage analysis as a means to in vivo "separation" of primary electrogenic and coupled secondary transport. *In:* Molecular and Cellular Aspects of Calcium in Plant Development. pp. 409–410. A. Trewavas, editor. Plenum, New York

Blatt, M.R., Slayman, C.L. 1987. Role of "active" potassium transport in the regulation of cytoplasmic pH by non-animal cells. *Proc. Natl. Acad. Sci. USA* **84:**2737–2742

Bowman, B., Slayman, C.W. 1979. The effects of vanadate on the plasma membrane ATPase of *Neurospora crassa*. *J. Biol. Chem.* **254:**2928–2934

Chapman, J.B., Johnson, E.A., Kootsey, J.M. 1983. Electrical and biochemical properties of an enzyme model of the sodium pump. *J. Membrane Biol.* **74:**139–153

Cheeseman, J., LaFayette, P., Gronewald, J., Hanson, J. 1980. Effect of ATPase inhibitors on cell potential and K^+ influx in corn roots. *Plant Physiol.* **65:**1139–1145

Clint, G.M. 1985. The investigation of stomatal ionic relations using guard cell protoplasts. I. Methodology. *J. Exptl. Bot.* **36:**1726–1738

Eisenberg, R., Barcilon, V., Mathias, R. 1979. Electrical properties of spherical analysis. *Biophys. J.* **25:**151–180

Eisenberg, R., Engel, E. 1970. The spatial variation of membrane potential near a small source of current in a spherical cell. *J. Gen. Physiol.* **55:**736–757

Eisenberg, R.S., Johnson, E.A. 1970. Three-dimensional electrical field problems in physiology. *Prog. Biophys. Mol. Biol.* **20:**1–65

Felle, H. 1981. A study of the current-voltage relationships of electrogenic active and passive membrane elements in *Riccia fluitans*. *Biochim. Biophys. Acta* **646:**151–160

Felle, H. 1982. Effects of fusicoccin upon membrane potential, resistance and current-voltage characteristics in root hairs of *Sinapsis alba*. *Plant Sci. Lett.* **25:**219–225

Gepstein, S., Jacobs, M., Taiz, L. 1982. Inhibition of stomatal opening in *Vicia faba* epidermal tissue by vanadate and abscisic acid. *Plant. Sci. Lett.* **28:**63–72

Goffeau, A., Slayman, C.W. 1981. The proton translocating ATPase of the fungal plasma membrane. *Biochim. Biophys. Acta* **639:**197–223

Goldsmith, T., Goldsmith, M.-H. 1978. The interpretation of intracellular measurements of membrane potential, resistance, and coupling in cells of higher plants. *Planta* **143:**267–274

Gradmann, D. 1975. Analog circuit of the *Acetabularia* membrane. *J. Membrane Biol.* **25:**183–208

Gradmann, D., Hansen, U.-P., Long, W., Slayman, C.L., Warnke, J. 1978. Current-voltage relationships for the plasma membrane and its principal electrogenic pump in *Neurospora crassa*: I. Steady-state conditions. *J. Membrane Biol.* **29:**333–367

Gradmann, D., Hansen, U.-P., Slayman, C.L. 1982. Reaction kinetic analysis of current-voltage relationships for electrogenic pumps in *Neurospora* and *Acetabularia*. *Curr. Topics Membr. Transp.* **16:**257–281

Hansen, U.-P., Gradmann, D., Sanders, D., Slayman, C.L. 1981. Interpretation of current-voltage relationships for "active" ion transport systems. I. Steady-state reaction-kinetic analysis of class-I mechanisms. *J. Membrane Biol.* **63:**165–190

Hansen, U.-P., Slayman, C.L. 1978. Current-voltage relationships for a clearly electrogenic cotransport system. *In:* Membrane Transport Processes. Vol. 1, pp. 141–154. J. Hoffman, editor. Raven, New York

Hansen, U.-P., Tittor, J., Gradmann, D. 1983. Interpretation of current-voltage relationships for "active" ion transport systems: II. Nonsteady-state reaction-kinetic analysis of class-I mechanisms with one slow-time constant. *J. Membrane Biol.* **75:**141–169

Hodgkin, A.L., Katz, B. 1949. The effect of sodium ions on the electrical activity of the giant axon of the squid. *J. Physiol. (London)* **108:**37–77

Jack, J.J.B., Noble, D., Tsien, R.W. 1983. Electric Current Flow in Excitable Cells. Clarendon, Oxford

Kishimoto, U. Kami-ike, N., Takeuchi, Y., Ohkawa, T. 1984. A kinetic analysis of the electrogenic pump of *Chara corallina*: I. Inhibition of the pump by DCCD. *J. Membrane Biol.* **80:**175–183

Köhler, K., Bentrup, F.-W. 1983. The effect of fusaric acid upon electrical membrane properties and ATP level in photoautotrophic cell suspension cultures of *Chenopodium rubrum* L. *Z. Pflanzenphysiol.* **109:**355–361

Läuger, P., Stark, G. 1970. Kinetics of carrier-mediated ion transport across lipid bilayer membranes. *Biochim. Biophys. Acta* **211:**458–466

Lew, R., Spanswick, R.M. 1984. Characterization of the electrogenicity of soybean roots. *Plant Physiol.* **75:**1–6

MacRobbie, E.A.C. 1981. Effects of ABA in 'isolated' guard cells of *Commelina communis* L. *J. Exptl. Bot.* **32:**563–572

MacRobbie, E.A.C. 1983. Effects of light/dark on cation fluxes in guard cells of *Commelina communis* L. *J. Exptl. Bot.* **34:**1695–1710

MacRobbie, E.A.C. 1987. Stomatal guard cells. *In:* Ion Trans-

port in Plant Cells and Tissues. J. Hall and D.A. Baker, editors. Pitman, London (*in press*)

Marquardt, D. 1963. An algorithm for least-squares estimation of nonlinear parameters. *J. Soc. Ind. Appl. Math.* **11**:431–441

Mercier, A.J., Poole, R.J. 1980. Electrogenic pump activity in red beet: Its relation to ATP levels and to cation influx. *J. Membrane Biol.* **55**:165–174

Nakao, M., Gadsby, D.C. 1986. Voltage dependence of Na^+ translocation by the Na^+/K^+ pump. *Nature (London)* **323**:628–630

Noble, D. 1962. The voltage dependence of the cardiac membrane conductance. *Biophys. J.* **2**:381–393

Outlaw, W. 1983. Current concepts on the role of potassium in stomatal movements. *Physiol. Plant.* **59**:302–311

Palevitz, B., Hepler, P. 1985. Changes in dye coupling of stomatal cells of *Allium* and *Commelina* demonstrated by microinjection of Lucifer yellow. *Planta* **164**:473–479

Poole, R. 1978. Energy coupling for membrane transport. *Annu. Rev. Plant Physiol.* **29**:437–460

Press, W., Flannery, B., Teukolsky, S., Vetterling, W. 1986. Numerical recipies: The art of scientific computing. Cambridge University Press, Cambridge

Raschke, K. 1979. Movements of stomata. *In:* Encyclopedia of plant physiology, N.S. Movements of Plants. Vol. 7, pp. 383–441. W. Haupt and M.-E. Feinleib, editors. Springer, Berlin

Raschke, K., Humble, G. 1973. No uptake of anions required by opening stomata of *Vicia faba:* Guard cells release hydrogen ions. *Planta* **115**:47–57

Roberts, J.K.M., Lane, A., Clark, R., Nieman, R. 1985. Relationships between rate of synthesis of ATP and the concentrations of reactants and products of ATP hydrolysis in maize root tips, determined by ^{31}P-NMR. *Arch. Biochem. Biophys.* **240**:712–722

Roberts, J.K.M., Wemmer, D., Jardetsky, O. 1984. Measurements of mitochondrial ATPase activity in maize root tips by saturation transfer ^{31}P-NMR. *Plant Physiol.* **74**:632–639

Saftner, R., Raschke, K. 1981. Electrical potentials in stomatal complexes. *Plant Physiol.* **67**:1124–1132

Sanders, D., Hansen, U.-P., Slayman, C.L. 1981. Role of the plasma membrane proton pump in pH regulation in non-animal cells. *Proc. Natl. Acad. Sci. USA* **78**:5903–5907

Sanders, D., Slayman, C.L. 1982. Control of intracellular pH: Predominant role of oxidative metabolism, not proton transport, in the eukaryotic microorganism *Neurospora*. *J. Gen. Physiol.* **80**:377–402

Schroeder, J., Hedrich, R., Fernandez, J. 1984. Potassium-selective single channels in guard cell protoplasts of *Vicia faba*. *Nature (London)* **312**:361–363

Scott, I.R., Ellar, D.J. 1978. Metabolism and the triggering of germination of *Bacillus megaterium*. *Biochem. J.* **174**:627–634

Shimazaki, K., Gotow, K., Sakaki, T., Kondo, N. 1983. High respiratory activity of guard cell protoplasts from *Vicia faba* L. *Plant Cell Physiol.* **24**:1049–1056

Shimazaki, K., Gotow, K., Kondo, N. 1982. Photosynthetic properties of guard cell protoplast from *Vicia faba* L. *Plant Cell Physiol.* **23**:871–879

Shimazaki, K., Iino, M., Zeiger, E. 1986. Blue light-dependent proton extrusion by guard-cell protoplasts of *Vicia faba*. *Nature (London)* **319**:324–326

Slayman, C.L. 1965. Electrical properties of *Neurospora crassa:* Respiration and the intracellular potential. *J. Gen. Physiol.* **49**:93–116

Slayman, C.L., Long, W., Lu, C.Y.-H. 1973. The relationship between ATP and an electrogenic pump in the plasma membrane of *Neurospora crassa*. *J. Membrane Biol.* **14**:305–338

Slayman, C.L., Sanders, D. 1985. Steady-state kinetic analysis of an electroenzyme. *Symp. Soc. Biochem.* **50**:11–29

Smith, J.R. 1984. The electrical properties of plant cell membranes. II. Distortion of non-linear current-voltage characteristics induced by the cable properties of *Chara*. *Aust. J. Plant Physiol.* **11**:211–224

Smith, J.R., Walker, N.A. 1983. Membrane conductance of *Chara* measured in the acid and basic zones. *J. Membrane Biol.* **73**:193–202

Sokolik, A.I., Yurin, V.M. 1986. Potassium channels in plasmalemma of *Nitella* cells at rest. *J. Membrane Biol.* **89**:9–22

Spanswick, R.M. 1981. Electrogenic ion pumps. *Annu. Rev. Plant. Physiol.* **32**:267–312

Swarup, G., Speeg, V., Cohen, S., Garbers, D. 1982. Phosphotyrosyl-protein phosphatase of TCRC-2 cells. *J. Biol. Chem.* **257**:7298–7301

Sze, H. 1985. H^+-translocating ATPases. *Annu. Rev. Plant Physiol.* **36**:175–208

Takeshige, K., Shimmen, T., Tazawa, M. 1986. Quantitative analysis of ATP-dependent H^+ efflux and pump current driven by an electrogenic pump in *Nitellopsis obtusa*. *Plant Cell Physiol.* **27**:337–348

Takeuchi, Y., Kishimoto, U., Ohkawa, T., Kami-ike, N. 1985. A kinetic analysis of the electrogenic pump of *Chara corallina:* II. Dependence of the pump activity on external pH. *J. Membrane Biol.* **86**:17–26

Tracey, A., Gresser, M. 1986. Interaction of vanadate with phenol and tyrosine: Implications for the effects of vanadate on systems regulated by tyrosine phosphorylation. *Proc. Natl. Acad. Sci. USA* **83**:609–613

Tyerman, S.D., Findlay, G.P., Paterson, G.J. 1986. Inward membrane current in *Chara inflata*. I. A voltage- and time-dependent Cl^- component. *J. Membrane Biol.* **89**:139–152

Walker, N.A., Smith, F.A. 1975. Intracellular pH in *Chara corallina* measured by DMO distribution. *Plant Sci. Lett.* **4**:125–132

Wille, A., Lucas, W. 1984. Ultrastructural and histochemical studies on guard cells. *Planta* **160**:129–142

Zeiger, E. 1983. The biology of stomatal guard cells. *Annu. Rev. Plant Physiol.* **34**:441–475

Received 31 March 1987; revised 15 June 1987

Appendix

Current Conduction and Voltage Profiles within Guard Cells

Knowing the distribution of current passed within the cell presents a fundamental obstacle to analysis of *I-V* measurements from higher plants. The problem arises primarily because of uncertainties about the size and shape of the cells, and because of intercellular coupling via plasmadesmata (*cf.* Goldsmith & Goldsmith, 1978; Spanswick, 1981). Currents passed from a "point source"—a single, intracellular microelectrode—may be distrib-

Table A1. Steady-state voltage decrement in *Vicia* guard cells[a]

Cell	V_m /mV	G_m /S m^{-2}	V_0 /mV	ΔV_0 /mV	ΔV_x /mV	$\Delta V_x/\Delta V_0$	λ /μm	l /μm	x /μm
1	−76.2	2.02	−291.5	−215.3	−213.9	0.993	295	38.7	12.7
			41.3	117.4	116.9	0.996			
2	−119.1	0.75	−297.4	−178.2	−177.5	0.996	472	43.4	20.3
			36.9	156.0	155.3	0.996			
3[b]	−131.8	0.60	−289.1	−157.2	−156.0	0.992	367	38.2	22.9
			44.2	176.0	173.8	0.988			
4	−81.8	0.33	−376.0	−294.2	−292.5	0.994	365	41.3	17.8
			35.4	117.2	116.7	0.996			

[a] Voltages at two separate points within single cells of length l recorded in double impalements. Cell potentials (V_0) clamped at steps (ΔV_0) from the free-running potential (V_m) using the two-electrode method and double-barrelled microelectrodes (Materials and Methods); a second (single-barrelled) microelectrode recorded voltage steps (ΔV_x) independently at a point (x) distant from the first. Clamp steps, 200-msec duration, run between −300 (−380, cell 4) and +50 mV. Raw data listed are for the voltage extremes, where spatial decrements would be most apparent. Space constants (λ) were calculated from Eq. (A1) for voltage steps over the "linear" portion of the *I-V* relation (*see* Fig. A2) to approx. ±50 mV from V_m. Both the ratio $\Delta V_x/\Delta V_0$ and large λ values relative to l emphasize the lack of any appreciable voltage gradient in the steady state.

[b] Cell *I-V* relation shown in Fig. A2.

uted nonuniformly, introducing temporal and spatial variations in the voltage, and bedeviling any quantitative description.

Even when temporal changes can be ignored, as in the case of steady-state measurements, spatial variations in current flow across the membrane must be a concern. Both *static* and *dynamic* features of the apparent membrane *I-V* relations are suspect in recordings with a single, voltage-following electrode. The bias is to linearize the intrinsic *I-V* characteristic and also to attenuate *changes* in the apparent *I-V* relations and membrane conductance (Noble, 1962; Jack, Noble & Tsien, 1983; Smith, 1984). As a result, not only is fine structure within the *I-V* characteristic lost but, in addition, it can become almost impossible to detect even large changes of membrane conductance (e.g. with experimental treatments) in the recorded input resistance.

These issues are unlikely to carry any weight for small, single cells with similar orthogonal dimensions, such as guard cells. Provided the membrane resistance is much greater than the internal resistivity—a situation typical of plant cells (*see* Smith & Walker, 1983; Smith, 1984)—the cell should behave electrically as a sphere. There are, however, occasions when current spread becomes important, even in spherical cells. Theoretically infinite current densities occur at a point source of injection. It follows that recordings using double-barrelled electrodes, or a single electrode with a bridge for current passing, might give erroneously high (theoretically infinite!) resistances by virtue of the recording position (Eisenberg & Engel, 1970; Eisenberg & Johnson, 1970; Eisenberg, Barcilon & Mathias, 1979; but *see* Blatt & Slayman, 1983). The problem is potentially magnified by the tonoplast and by uncertainties surrounding electrode placements between vacuole and cytoplasm (*but see* Blatt, 1987*a*).

To assess the magnitude of these problems for electrical measurements from the guard cells, I recorded the *I-V* characteristics using two separate electrodes in each of four cells. A double-barrelled microelectrode was used, as before, to pass current and to record voltage, and was placed near one end of the cell. At the same time, a single electrode was inserted toward the other end of the cell, and was used to record voltage only, independent of the voltage-clamp circuit (*see* Fig. 1). Current-voltage scans were carried out in the usual fashion, but with the addition that voltage samplings were taken from both ends of the cell with each pulse. For technical reasons, the time dependences of both voltage records and of the clamp current were not followed during these scans. The pulse width was increased (=200 msec) to insure that a near-steady state was achieved by the time of sampling at the end of each pulse, but later recordings showed this to be an unnecessary precaution (*see* Fig. A1).

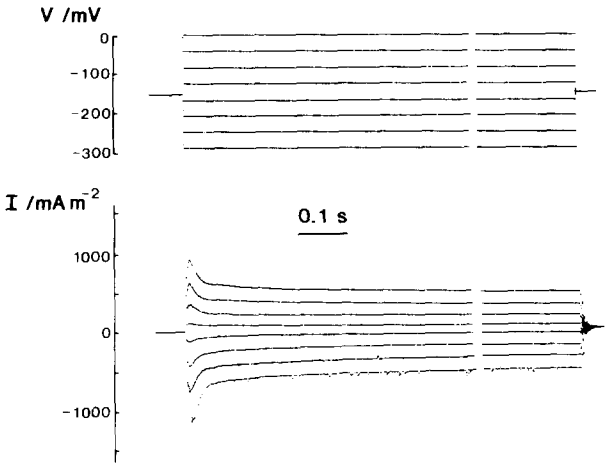

Fig. A1. Current and voltage records from a respiring guard cell during 1-sec long voltage-clamp pulses (600–800-msec interval compressed). The cell was clamped at eight potentials between 0 and −300 mV away from V_m (−154 mV). The current was filtered at 3 kHz (−3 dB), and current and voltage were recorded at 2-msec intervals. Capacitative spikes (with voltage steps) are clamp artifacts. Transients in clamp currents were generally evident during the first 10–50 msec and are likely of transport origin (*see* Hansen, Tittor & Gradmann, 1983; Nakao & Gadsby, 1986). Treatments with cyanide eliminated the early transients within the time frame for measurements (3–5 min, *not shown*)

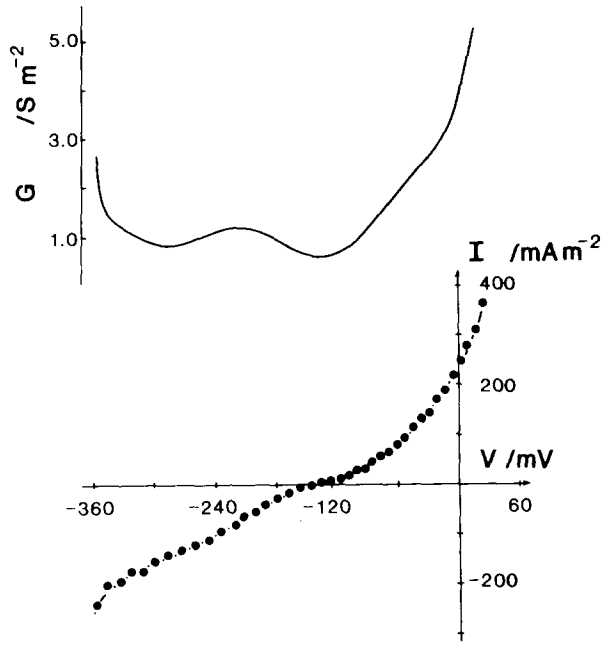

Fig. A2. Current- and conductance-voltage profiles for cell 3 in Table A1. Guard cell potentials were low in double impalements, but the *I-V* and *G-V* curves did indicate pump activity in cells 1–3. Note the pump G_{max} near −220 mV

Table A1 gives a synopsis of the results. In all four cells, the voltage steps (from the free-running potential) recorded by the two electrodes never differed by more than 2–3 mV, or roughly 0.8% of the clamped membrane potential. This discrepancy is close to the cumulative percentage errors in the gains of the amplifiers and sampling circuits (0.5%), suggesting that the membrane potentials at either end of each cell were very close, if not identical. Figure A2 shows the *I-V* profile obtained during a single voltage-clamp scan from one cell. Free-running potentials from the four cells were more positive than similar recordings made with single impalements, and probably indicated some detrimental effects of multiple penetration; but membrane conductances scattered about the normal range. So, inhomogeneities in current spread could not have lead to any serious distortion of the guard cell *I-V* relations.

[With steady-state measurements of voltage at two known points, relative to the point of current injection, it is possible to estimate the space constant for a cell. Table A1 includes, also, the results of these calculations which, again, emphasize the "spherical" electrical geometry of the guard cells. For this purpose, the cell dimensions were approximated by a cylinder, truncated at either end by open circuits. The steady-state voltage decrement $\Delta V_x/\Delta V_0$ at position x along the cell, resulting from a current injected at a point ($x = 0$), can be derived from linear cable theory (Jack et al., 1983) as

$$\Delta V_x/\Delta V_0 = \frac{\cosh[(l - x)/\lambda]}{\cosh(l/\lambda)} \quad \text{(A1)}$$

where ΔV_x and ΔV_0 are the steady-state voltage displacements from V_m at positions x and $x = 0$, respectively, and λ is the space constant for the cell of length l. Calculations using this equation were carried out for voltage pulses near the free-running potentials, where the *I-V* profile was roughly linear; for the sake of argument, also, I took the voltage steps (ΔV_x, ΔV_0) from the electrode pairs as recorded. Values for λ were found by successive approximation using a simplified Newton-Raphson algorithm (Press et al., 1986). The figures quoted are means, from within each *I-V* scan, of 6–8 separate clamp steps for which $\Delta V_x/\Delta V_0 < 1$, and should be regarded as minimum estimates only.]